COMPDYN 2011
III ECCOMAS Thematic Conference on
Computational Methods in Structural Dynamics and Earthquake Engineering
M. Papadrakakis, M. Fragiadakis, V. Plevris (eds.)
Corfu, Greece, 25–28 May 2011

FINITE ELEMENT ANALYSIS OF BURIED STEEL PIPELINES UNDER STRIKE-SLIP FAULT DISPLACEMENTS

Polynikis Vazouras[1], Spyros A. Karamanos[2], and Panos Dakoulas[1]

[1] Department of Civil Engineering
University of Thessaly, Volos 38334, Greece
e-mail: pvazour@yahoo.gr; dakoulas@uth.gr

[2] Department of Mechanical Engineering
University of Thessaly, Volos 38334, Greece
e-mail: skara@uth.gr; www.mie.uth.gr/karamanos.htm

Keywords: Pipeline, Buckling, Seismic fault, Finite elements, Pipeline integrity.

Abstract. *The present paper investigates the mechanical behaviour of buried steel pipelines, crossing active strike-slip tectonic faults. The fault plane is vertical and crosses the pipeline axis at a certain angle. The interacting soil-pipeline system is modelled rigorously through finite elements, which account for large strains and displacements, nonlinear material behaviour and special conditions of contact and friction on the soil-pipe interface. Steel pipelines of various diameter-to-thickness ratios, and typical steel material for pipeline applications (API 5L grades X65 and X80) are considered. Most of the numerical results in the paper refer to the case where the fault plane crosses the pipeline axis at right angle. In particular, the paper investigates the effects of various soil and pipeline parameters on the mechanical response of the pipeline, with particular emphasis on pipe wall failure due to "local buckling" or "kinking" and pipe wall rupture. The effects of shear soil strength and stiffness are also investigated. Furthermore, the influence of the presence of pipeline internal pressure on the mechanical response of the steel pipeline is examined. Numerical results aim at determining the fault displacement at which the pipeline failure occurs, and they are presented in a graphical form that shows the critical fault displacement, the corresponding critical strain versus the pipe diameter-to-thickness ratio. Furthermore, results for cases where the fault plane crosses the pipeline axis at an angle different that 90-degress are presented and the corresponding failure modes are identified. It is expected that the results of the present study can be used for efficient pipeline design in cases where active faults are expected to impose significant ground-induced deformation to the pipeline.*

1 INTRODUCTION

Seismic events constitute a threat for buried pipeline structural integrity. In particular, permanent ground deformation applied on the pipeline in a quasi-static manner, and not necessarily associated with high seismic intensity, may cause serious pipeline damages, reported in numerous earthquakes, such as the 1995 Kobe earthquake [1], the 1999 Kocaeli earthquake [2] and the 1999 Chi-Chi earthquake [3].

The present paper focuses on the mechanical response of continuous (welded) buried steel pipelines crossing active strike-slip seismic faults, a particular ground-induced action, associated with axial, shear and bending loads. High stresses and strains are developed in critical locations, which are well into the inelastic range of pipe material and may cause pipeline failure. In particular, high tensile stresses may cause fracture of the pipeline wall, especially at welds or defected locations, whereas high compression stresses may cause buckling, mainly in the form of pipe wall wrinkling, a shell-type instability, referred to as "local buckling" or "kinking".

Newmark and Hall [4] were the first to attempt prediction of pipeline mechanical response under fault displacement, using a simplified analytical model of a long cable with small displacements. Their work has been extended by Kennedy et al. [5] [6] considering non-uniform friction between the pipe and the surrounding soil, and further enhanced by Wang and Yeh [7] to account for pipeline bending stiffness. Notable analytical works on the subject, based on a beam-type approach for pipeline modelling have been presented by Vougioukas et al. [8], Wang and Wang [9] and Takada et al. [10]. Kokavessis and Anagnostidis [11], presented a finite element methodology to simulate buried pipeline behaviour under permanent ground-induced actions, using contact elements to describe the soil-pipe interaction. Furthermore, Karamitros et al. [12] presented an enhanced analytical beam-type methodology, supported by three-dimensional finite element models, which employed shell elements for describing the pipe and nonlinear springs to simulate soil behavior. Liu et al. [13] presented a numerical simulation of pipelines crossing active faults through a combination of shell elements and springs, similar to the model in [12].

Experimental works on the effects of strike-slip faults on buried polyethylene (HDPE) pipelines have been reported by Ha et al. [14][15] and Abdoun et al. [16], based on centrifuge modelling of pipeline response and examined the influence of the type of faulting, the angle of strike-slip faults on the pipeline mechanical behaviour, as well as the effects of buried depth, pipeline diameter, and moisture content.

The work in the present paper is part of an extensive research effort aimed at investigating the response of buried steel pipelines crossing active faults for various soil conditions, using advanced numerical simulation tools and identifying possible failure modes, with emphasis on site conditions (i.e. the properties of the surrounding soil). The present work follows an integrated approach, which is based on modelling of the soil-pipeline system through nonlinear finite elements, accounting rigorously for (a) the inelastic behaviour of the surrounding soil, (b) the interaction and the contact between the soil and the pipe (including friction contact and the development of gap), (c) the development of large inelastic strains in the steel pipeline, (d) the distortion of the pipeline cross-section and possible local buckling formation, (e) the presence of internal pressure. The pipeline axis is assumed horizontal and crosses the fault plane at right angle. Considering a variety of soil parameters for both cohesive and non-cohesive soils, the influence of soil conditions on the pipeline structural response is examined in detail. Furthermore, the effects of pipeline diameter-to-thickness ratio D/t and steel material on pipeline response are also investigated. The numerical results are employed to develop inter-

action diagrams of the fault displacement causing pipeline failure with respect to the value of pipe diameter-to-thickness ratio D/t, which could be used for practical design purposes.

2 NUMERICAL MODELING

General-purpose finite element program ABAQUS [18] is employed to simulate the mechanical behavior of the steel pipe, the surrounding soil medium and their interaction in a rigorous manner, considering the nonlinear geometry of the soil and the pipe (including the cross-sectional distortions of the pipeline cross-section), through a large-strain description of the pipeline-soil system and the inelastic material behavior for both the pipe and the soil.

Figure 1 shows the elongated prismatic model considered for simulating this permanent ground-induced action, where the pipeline is embedded in the soil. The corresponding finite element mesh for the soil formation is depicted in Figure 1a and Figure 1b, and for the steel pipe in Figure 1c. Four-node reduced-integration shell elements (type S4R) are employed for modeling the pipeline cylinder, whereas eight-node reduced-integration "brick" elements (C3D8R) are used to simulate the surrounding soil. The top surface represents the soil surface, and the burial depth is chosen equal to about 2 pipe diameters, which is in accordance with pipeline engineering practice. A short parametric study demonstrated that a 60-diameter length of the pipeline (in the x direction) is adequate for the purposes of the present analysis. Furthermore, prism dimensions in directions y, z equal to 10 and 5 times the pipe diameter, respectively, are also found to be adequate. The seismic fault plane crosses the pipeline axis at a certain angle and divides the soil in two equal parts (Figure 1a). The analysis is conducted in two steps; gravity loading is applied first and, subsequently, fault movement is imposed. The vertical boundary nodes of the first block remain fixed in the horizontal direction (including the end nodes of the steel pipeline), whereas a uniform horizontal displacement due to fault movement is imposed in the external nodes of the second (moving) block (including the end nodes of the pipeline). A finer mesh was employed for the central part of the pipeline, where maximum stresses and strains are expected, with a total of 54 shell elements around the cylinder circumference in this central part, whereas the size of the shell elements in the longitudinal direction has been chosen equal to 1/26 of the pipeline outer diameter D.

Figure 2a plots the soil – pipeline system after a seismic fault movement, for a plane perpendicular to the pipeline axis. The fault movement is considered to occur within a narrow transverse zone of width w, to avoid discontinuity at the vicinity of the fault, which sometimes causes numerical problems and corresponds to a more realistic representation of the fault displacement mechanism. Following a short parametric study, the value of w has been considered equal to 0.33 m.

A large-strain J_2 flow (von Mises) plasticity model, with isotropic hardening is employed to describe the mechanical behavior of the steel pipe material, calibrated through an appropriate uniaxial stress-strain curve from a tensile test. Furthermore, an elastic-perfectly plastic Mohr-Coulomb model is considered for the soil behavior, characterized by the soil cohesiveness c, the friction angle ϕ, the elastic modulus E, and Poisson's ratio v. The dilation angle ψ is assumed to be equal to zero throughout this study. A contact algorithm is considered to simulate the interface between the outer surface of the steel pipe and the surrounding soil, which takes into account interface friction, which is considered through definition of an appropriate friction coefficient μ. In our analysis, the value of μ is equal to 0.3. Moreover, the interface allows separation of the pipe and the surrounding soil. The analysis proceeds using a displacement-controlled scheme, which increases gradually the fault displacement d. At each increment of the nonlinear analysis, stresses and strains at the pipeline wall are recorded.

3 NUMERICAL RESULTS

Using the above numerical simulation tools, results are obtained for steel pipelines for various values of the diameter-to-thickness ratio, as well as for different soil conditions. In all cases considered in the present paper, the outer pipe diameter of the pipe D is assumed equal to 914.4 mm (36 in), whereas the pipe wall thickness ranges from 6.35 mm (¼ in) to 19.05 mm (¾ in), so that a range of D/t values between 48 and 144 is covered. This range of D/t values is typical for onshore applications (oil, gas or water pipelines). The surrounding soil has dimensions 60m×10m×5m in directions x, y, z respectively.

In sections 3.1, 3.2 and 3.3, the seismic fault plane is perpendicular to the pipeline axis and located at the middle cross-section of the pipeline. Particular emphasis is given on the effects of external pressure on the structural response. Both X65 pipelines and high-strength steel X80 pipelines are analyzed. Finally, in section 3.4, numerical results are obtained for an X65 pipeline where the fault plane crosses the pipeline axis at angles different that 90-degress, aiming at identifying the corresponding failure modes.

3.1 X65 steel pipelines in cohesive soils

A moderately thick-walled X65 pipeline is considered first, with diameter and thickness equal to 914.4 mm (36 in) and 12.7 mm (0.5 in) respectively, so that D/t =72. The API 5L X65 steel material is a typical steel material for oil and gas pipeline applications, with a nominal stress-engineering strain curve shown with solid line in Figure 3a, obtained from a uniaxial tensile test. The yield stress σ_y is equal to 450 MPa (65 ksi) followed by a plastic plateau up to 3% strain and a strain-hardening regime with a hardening modulus equal to about $E_s/300$, where E_s is the Young's modulus of the steel material. Assuming a safety (reduction) factor equal to 0.72 [21], the maximum operating pressure $p_{\max}$ of this pipeline [$p_{\max} = 0.72 \times \left(2\sigma_y\, t/D\right)$] can be readily calculated equal to 9 MPa (90 barr).

The pipeline is assumed to be imbedded in a cohesive soil and to be crossing a fault zone having a width w equal to 0.33 m. At this stage, the internal pressure p is equal to zero, and a soft-to-firm clay is considered, referred to as Clay I, which under "undrained" loading conditions has a cohesion c = 50 kPa, friction angle $\varphi = 0^\circ$, Young's modulus E = 25 MPa and Poisson's ratio ν = 0.5. Figure 4a depicts the shape of the deformed pipeline at fault displacements d = 1 m, 2 m, 3 m and 4 m in the area near the fault. Moreover, Figure 4b depicts the shape of the deformed pipeline and the distribution of the longitudinal normal strain ε_x on its outer surface at fault displacement equal to d = 1 m and d = 4 m. The deformed shape of the pipeline at d = 1 m shows a localized deformation at point A, referred to as "local buckling" or "kinking", whereas point A is the "critical location" of the pipeline, at a distance of 5.45 m from the fault. Due to the skew-symmetry of the problem, a similar local deformation pattern occurs at point B, on the hidden side of the pipeline. Under increasing fault movement, a substantial development of this localized deformation pattern is observed, associated with the distortion of a significant part of the pipeline around this area, as shown in
Figure 4b, for a fault displacement of d = 4 m. As the pipeline length increases with continued fault movement, it results to higher tensile and smaller compressive strains in the longitudinal direction. Figure 4b, shows that for a fault displacement of d = 4 m compressive longitudinal strains are significantly lower than those corresponding to a fault displacement of d = 1 m.

Figure 5 shows the deformed shape of the pipeline at fault displacements d equal to 1 m, where a localized buckling pattern develops where the compressive stresses and strains reach a maximum value. It is also important to notice that, upon local buckling formation, the deformation of the pipeline localizes in the vicinity of the buckle, as shown in Figure 5b. The variations of longitudinal compressive and tensile strain ε_x along the two outer (most stressed) generators of the pipe cylinder are shown in Figure 6 and Figure 7 for different values of the fault displacement and for a small segment of the pipeline about the critical area. The results for the compressive strain shown in detail in Figure 6b, indicate that for a value of fault displacement greater than 0.67 m, significant distortion of the cross-section occurs due to the development of a localized wrinkling pattern (local buckling) on the pipe wall, on the compression side of the deformed pipeline. This stage is considered as the onset of local buckling.

One may notice that the value of fault displacement at which onset of localized buckling occurs (d_{cr}), referred to as "critical fault displacement", can be defined in many ways. In the present work, the onset of local buckling is considered at the stage where outward displacement of the pipe wall starts at the area of maximum compression. At that stage, bending strains due to pipe wall wrinkling develop (Figure 6), associated with significant tensile strains at the "ridge" of the buckle, so that the longitudinal compressive strains at this location at the outer surface of the pipe wall start decreasing, forming a short wave at this location. In the present case, this stage corresponds to a fault displacement equal to 0.67m as shown in Figure 6b.

At the above stage of local buckling onset, the longitudinal strain at the location of the buckle (ε_{cr}) is measured equal to 7.7×10^{-3} .Furthermore, at this critical buckling stage, the maximum tensile strain on the opposite side of the pipe ($\varepsilon_{T,\max}$) is 5.2×10^{-3}, which is much less than the strain that would cause tensile failure in the form of rupture in a non-seriously-defected pipeline [22]. It is noted that the formation of a local buckle is undesirable because it is associated with the concentration of strain at the buckled area, which may lead to fatigue cracking under repeated loading [23]. Upon formation of the local buckle, pipe deformation concentrates around the buckled cross-section. However, further continuation of the imposed deformation results in significant tensile strains at the buckled area, decreasing the compressive strains and resulting in high local tensile stresses, on either side of the pipeline cross-section, may lead to local fracture at welds or other locations where minor defects exist.

The effects of internal pressure on pipeline mechanical behavior are investigated by considering internally pressurized pipelines imbedded in the same soil conditions (Clay I). Numerical results corresponding to a pressure level of 50 barr, which is equal to 56% of the maximum operating pressure $p_{\max}$ indicate that, despite the fact that the buckled shapes of pressurized cylinders are similar to the buckled shape of Figure 5, the corresponding values of critical fault displacement d_{cr} and the compressive strain along the critical generator of the steel pipeline are somewhat lower than the ones shown in Figure 6b. Those results indicate that, in the case of buried (confined) pipes, the presence of internal pressure results in a decrease of critical fault displacement. The decrease is attributed to the development of additional stresses and strains in the pipeline wall that cause early yielding and lead to a premature local buckling failure. For the case of $p/p_{\max}$ =0.56, the maximum strain ε_{cr} at buckling (critical strain) is equal to 8.3×10^{-3}, which is similar yet slightly higher than the critical strain for zero pressure.

The numerical results in Figure 8 and in Figure 9 refer to an X65 steel pipeline with D/t ratio equal to 72, buried in stiffer cohesive soil conditions. The values of soil parameters c, E and φ are equal to 200 kPa, 100 MPa and 0^o, respectively, and correspond to a stiff clay under "undrained conditions", referred to as Clay II. The width of the fault zone is equal to 0.33 m. The numerical results indicate that pipe bending deformation in the stiff soil occurs within a shorter distance from the fault location, and the critical area is at 3.2 m from the fault. Comparison of those results with the results shown in Figures 6 and 7 demonstrates the significant effect of site conditions on the mechanical behavior of the steel pipeline. In other words, for the same fault displacement d, higher bending stresses and strains occur in the case of a stiff soil than those in the case of a soft soil. The numerical verification of the above observation is offered in Figure 8 and Figure 9, which depict the variation of longitudinal (axial) normal strain along the compression generator. Local buckling occurs when the fault displacement becomes equal to 0.23 m, which is much less than the corresponding critical fault displacement for the case of soft clay (0.67 m). The corresponding maximum compressive strain ε_{cr} that causes local buckling is equal to 7.3×10^{-3}, whereas the maximum tensile strain $\varepsilon_{T,\max}$ along the opposite generator at the stage of local buckling onset is equal to 4.8×10^{-3}. The striking difference between softer and stiffer soil conditions is attributed to the fact that a steel pipeline in a softer soil, when subjected to a fault displacement, accommodates itself easier within the deformable soil, resulting in lower bending stresses and strains, which enable the pipeline to sustain larger ground-imposed displacements.

To investigate the effects of the diameter-to-thickness D/t ratio in cohesive soils (Clay I, II), numerical results are obtained for 36-inch-diameter X65 steel pipelines with thickness ranging between ¼-inch and ¾-inch, corresponding to D/t values between 48 and 144.

The numerical results are summarized in Figure 10. In particular, Figure 10a plots the fault critical displacement, d_{cr}, normalized by the pipe diameter D, in terms of the diameter-to-thickness ratio, D/t. The results show a substantial decrease of d_{cr} with increasing value of the D/t ratio, which means that thin-walled pipelines are more prone to buckling and fail at relatively small values of fault displacement. Furthermore, stiff soil conditions result in significantly lower deformation capacity of the pipeline. In Figure 10b the corresponding critical compressive strain at the onset of local buckling, ε_{cr}, is plotted against the value of the diameter-to-thickness ratio, D/t. The results indicate that thinner pipes buckle at smaller critical strain, which is in accordance with test data and numerical results from non-confined pipes [24].

In the above results, no critical displacement or critical strain is shown for $D/t = 44$ and soft soil conditions (Clay I). In this particular case, the numerical results did not indicate local buckling; the pipeline exhibited significant ground-induced deformation without any wrinkling of the pipeline wall for fault displacements that exceed 2.5 m. The significant tensile strains developed in the pipeline due to longitudinal pipeline stretching, after a certain fault movement, are responsible for this behavior.

In Figure 10, the effects of internal pressure are also depicted. The numerical results are obtained for a pressure level equal to 56% of the maximum operating pressure, $p_{\max}$, and show that the presence of internal pressure results to a small decrease of critical fault movement, d_{cr} in Figure 10a, due to the additional stresses and strains in the pipeline wall because of pressure. Furthermore, the corresponding critical strain in the presence of pressure is similar to the corresponding critical strain for the zero pressure case, as shown in Figure 10b.

3.2 X65 steel pipelines in non-cohesive soils

The response of an X65 steel pipeline with D/t = 72 embedded in non-cohesive soils is examined, by considering representative results for two frictional soils and comparing them to those obtained for the cohesive soils. First, a granular soil is considered with a friction angle φ=30^o, Young's modulus E=8 MPa and Poisson's ratio ν=0.3, corresponding to loose sand and referred to as "Sand I". The relatively small value of the stress-depended Young's modulus E is justified by the shallow embedment depth of the pipeline. A small amount of artificial cohesion equal to c = 5 kPa was also included to prevent numerical difficulties associated with the behavior of a purely frictional material at very small confining stress, such as in the case of a gap opening at the pipe-soil interface. Figure 11 and Figure 12 show the variation of the axial strain ε_x along the compression and tension outer sides, respectively, of the buckled area for Sand I. The critical distance from the fault, corresponding to the point with maximum bending curvature along the pipe, is 6.1 meters. The results for the compressive strain shown in Figure 11 indicate that at a value of fault displacement equal to 0.87 m, local buckling occurs, and beyond this stage, significant distortion of the cross-section occurs due to local buckling on the pipe wall on the compression side of the bent pipeline. The shape of the developing buckling is similar to that of Clay I. The longitudinal strain at the location of the buckle (ε_{cr}) is equal to 9.7×10^{-3}. Furthermore, at the critical buckling stage (d=0.87 m), the maximum tensile strain on the opposite side of the pipe ($\varepsilon_{T,\max}$) is 6.8×10^{-3}, which is much less than the strain that would cause tensile rupture. Beyond the formation of the local buckle, pipe deformation concentrates around the buckled cross-section and the localized wrinkling pattern is further developed. Further continuation of the imposed deformation results in pipe-wall folding, which is accompanied by significant local strains (compressive and tensile) at the buckled area. Moreover, the maximum tensile strain on the opposite (tensile) side of the pipe is also significantly increased.

Similar results are obtained for an X65 steel pipeline with D/t = 72, embedded in a more dense sand with values of φ and E equal to 40^o and 50 MPa, respectively, referred to as "Sand II". The numerical results indicate that pipe bending deformation in Sand II occurs within a shorter distance from the fault location (5.1 m) due to the higher strength of this sand. Comparison of those results with the results in Figure 11 and Figure 12 demonstrates that for the same fault displacement d, higher bending stresses and strains occur in the case of Sand II. Furthermore, local buckling occurs when the fault displacement becomes equal to 0.70 m, which is less than the corresponding critical fault displacement for the case of loose sand (0.87 m). The maximum compressive strain ε_{cr} that causes local buckling is equal to 10.47×10^{-3}, whereas the corresponding maximum tensile strain $\varepsilon_{T,\max}$ along the opposite generator is equal to 6.98×10^{-3}.

Finally, the numerical results for the mechanical behavior of X65 pipelines in non-cohesive soils (Sand I and II) are summarized in Figure 13, in terms of the normalized fault critical displacement and the critical corresponding strain at buckling with respect to the diameter-to-thickness ratio, D/t. The results shown in Figure 13a indicate that dense soil conditions (sand II) result in lower deformation capacity of the pipeline.

3.3 Behavior of X80 steel pipelines

The behavior of buried high-strength steel (API X80) pipelines under normal fault-induced deformation is also analyzed, using the numerical tools described in the previous sections.

The nominal uniaxial tensile stress-strain relationship of the X80 material is plotted in Figure 3. The dashed material curve, which has a yield stress of 596 MPa and does not have a plastic plateau, corresponds to a cold expanded (UOE) pipe. The solid material curve with a yield stress of 550 MPa and a plastic plateau up to a strain of 1.48% represents a seamless steel pipe material. Results are obtained for 36-inch-diameter X80 steel pipelines with D/t ratios between 48 and 144. Figure 14a plots the value of the fault critical displacement, d_{cr}, normalized by the pipe diameter D, in terms of the diameter-to-thickness ratio, D/t, for the two types of X80 steel and for cohesive soil conditions (Clay I and II). As in the case of X65, the value of d_{cr} decreases significantly with increasing value of D/t, indicating that thin-walled pipelines are more vulnerable to buckling and may fail at relatively small values of fault displacement. It should be noted that for the softer Clay I material, no values of d_{cr} are given for D/t = 44 and 72, as no wrinkling of the pipeline wall was observed in this case even for fault displacements exceeding 4 m. This is attributed to the beneficial effect of tensile deformation on the mechanical behavior of those relatively thick pipes, as described in the Appendix. Naturally, the values of d_{cr} for the high-strength steel X80 pipes in Figure 14a are higher than those for the X65 pipes given in Figure 10a. Similarly, Figure 14b plots the corresponding critical axial strain, ε_{cr}, versus the diameter-to-thickness ratio, D/t, for zero internal pressure. Comparing the behavior of the two X80 materials, it is evident that both d_{cr} and ε_{cr} are higher for UOE pipe due to both increase of yield strength and higher initial post-yielding tangent modulus. The increase of buckling strength in UOE pipes is in accordance with the test data reported elsewhere [24].

3.4 Effects of the pipeline-fault crossing angle

In this section, a short parametric study is conducted to examine the effects of pipeline-fault crossing angle on the pipeline structural performance, as shown in Figure 15. The crossing angle β is the main parameter of interest; positive values of β correspond to geometries that induce tension in the pipeline, whereas negative values of β are dassociate with compression of the pipeline. A 36-inch-diameter, ½-inch-thick X65 pipeline, embedded in soft-to-firm clay soil conditions (Clay I), is examined for various crossing angles.

Figure 16 shows the deformed shape of the above pipeline for a value of β equal to 25 degrees, at a fault displacement d = 2 m. At this angle, local buckling does not occur. The deformed shape shows a significant distortion of the pipeline cross-section in the form of ovalization. The amount of ovalization, defined as $ov = \Delta D/D$ (where ΔD is the change of diameter in the plane of bending), reaches a limit value of 0.15 at fault displacement of 1 m, at the area where pipe intersects with the fault. It is noted that this value of 0.15 is specified by NEN 3650 specification, as described in [25]. Under increasing fault movement, this ovalization pattern is further developed resulting in a inversion of the pipeline wall (i.e. a local "concave" deformation pattern on the pipeline wall), for a fault displacement of d = 2.53 m. Critical tension strain (3%) appears at a fault displacement d = 0.64 m, whereas a maximum tensile strain of 5% occurs at a fault displacement d = 1.42 m, at a distance 1.1 m away from fault.

The deformed shape of the above 36-inch-diameter, ½-inch-thick X65 steel pipeline in Clay I soil conditions, crossing the fault plane at an angle of β equal to 45 degrees, is shown in Figure 17. The amount of ovalization reaches a critical value of 0.15 at fault displacement of 1.08 m, at the area where pipe intersects with the fault. With increasing fault displacement,

this ovalization pattern is further developed. For a fault displacement equal to 4 m no "inversion" of the pipeline wall has been observed. Critical tension strain (3%) is reached at a fault displacement d = 0.37 m, whereas a maximum tensile strain of 5% occurs at a fault displacement d = 1.14 m, at the point where pipeline crosses the fault plane.

The response becomes quite different if a opposite crossing angle is considered, corresponding to a negative value of β. In this case, fault motion is associated with a decrease of length of the pipeline, resulting in the development of significant compressive stresses and strains, leading to local buckling. In Figure 18, the deformed shape of the above 36-inch-diameter $\frac{1}{2}$-inch-thick X65 steel pipeline in Clay I soil conditions, crossing the fault plane at an angle of β equal to -10 degrees, is shown. The critical fault displacement has been computed equal to 34 cm. Upon continuation of fault displacement, the buckle pattern is further developed, so that an inversion of the pipeline wall occurs at fault displacement of 75 cm in the same cross- section where buckle appears. The cross- section where maximum deformation occurs is located 7.5 meters away from fault.

4 CONCLUSIONS

Using advanced finite element simulation tools, the mechanical behaviour of buried steel pipelines crossing an active strike-slip fault was investigated. The pipeline is assumed horizontal and normal to the fault plane, an idealized case, which allows for the investigation of several soil and pipe parameters on pipeline deformation and strength. In particular, the effects of various cohesive and non-cohesive soil conditions (expressed through various values of soil cohesion, friction and stiffness parameters (c, φ, E) on the structural response of the pipe are examined, with particular emphasis on pipe wall failure.

For pipelines crossing strike-slip faults at right angle, an extensive parametric study is conducted, and numerical results are obtained for various values of D/t ratio and for X65 and X80 steel pipelines. In the majority of the cases analyzed, it is shown that the formation of local buckling due to excessive compressive strains at the pipeline wall is the governing mode of failure. The numerical results are presented in diagram form for the critical fault displacement d_{cr} and the corresponding critical strain ε_{cr}, and indicate a strong dependence in terms of the pipeline diameter-to-thickness ratio D/t.

It is concluded that, for pipelines crossing strike-slip faults at right angle, in cohesive soils, softer ground conditions result in a large deformation capacity of the pipeline, whereas stiff ground conditions decrease the critical fault displacement. Similarly, in non-cohesive soils, loose sand conditions results in larger values of critical fault displacement than in dense soil conditions. The width of the fault slip zone was found to have non-important effects for the mechanical behaviour of the pipe. It was demonstrated that the presence of internal pressure results in a small decrease of the deformation capacity, due to early yielding of the steel material. It was also concluded that high-strength X80 steel pipelines have a greater deformation capacity than X65 pipelines. Furthermore, cold-formed UOE X80 pipes exhibit better behaviour in terms of buckling than seamless X80 pipes due to strain hardening. Furthermore, the numerical results show that thick-walled pipes may not exhibit buckling; in those pipelines wall fracture may occur due to the development of excessive tensile strains.

Finally, numerical results are obtained for pipelines crossing the vertical fault at angles different that 90-degress. In "negative" values of the angle, local buckling of the pipeline wall is the dominant mode of failure; local wrinkling increases with increasing fault displacement. On the other hand, for "positive" values of the crossing angle, the behaviour is considerably different. Local wrinkling does not occur; nevertheless the pipeline exhibits a significant dis-

tortion of its cross-section, followed by the development of significant tensile strains that may lead to pipeline rupture.

REFERENCES

[1] Nakata T, Hasuda K (1995). Active fault I 1995 Hyogoken Nanbu earthquake. *Kagaku* 1995; 65:127–142

[2] Earthquake Engineering Research Institute (1999). "Kocaeli, Turkey Earthquake of August 17", *EERI Special Earthquake Report*.

[3] Takada S, Nakayama M, Ueno J, Tajima C (1999). Report on Taiwan Earthquake, *RCUSS, Earthquake Lab. of Kobe University*; 2–9

[4] Newmark N. M., Hall W. J. (1975), "Pipeline design to resist large fault displacement". *Proceedings of U.S. National Conference on Earthquake Engineering*; 416–425.

[5] Kennedy, R. P., Chow, A. W. and Williamson, R. A. (1977), "Fault movement effects on buried oil pipeline", *ASCE Journal of Transportation Engineering*, Vol. 103, pp. 617-633.

[6] Kennedy R. P., Kincaid R. H. (1983). "Fault crossing design for buried gas oil pipelines". *ASME, PVP conference*; 77:1–9

[7] Wang, L. R. L. and Yeh, Y. A. (1985), "A refined seismic analysis and design of buried pipeline for fault movement", *Earthquake Engineering & Structural Dynamics*, Vol. 13, pp. 75-96.

[8] Vougioukas E. A., Theodossis, C., Carydis P. G. (1979), "Seismic analysis of buried pipelines subjected to vertical fault movement.", *ASCE Journal of Technical Councils*, Vol. 105(TCI), pp. 432– 441.

[9] Wang L. L. R., Wang L. J. (1995), Parametric study of buried pipelines due to large fault movement. *ASCE, TCLEE* 1995; (6):152–159.

[10] Takada, S., Hassani, N. and Fukuda, K. (2001), "A new proposal for simplified design of buried steel pipes crossing active faults", *Earthquake Engineering and Structural Dynamics*, 2001; Vol. 30: pp.1243–1257.

[11] Kokavessis, N. K. and Anagnostidis, G. S. (2006), "Finite Element Modelling of Buried Pipelines Subjected to Seismic Loads: Soil Structure Interaction Using Contact Elements.", *Proceedings, ASME PVP conference*, Vancouver, BC, Canada.

[12] Karamitros, D. K., Bouckovalas, G. D., and Kouretzis, G. P. (2007), "Stress Analysis of Buried Steel Pipelines at Strike-Slip Fault Crossings.", *Soil Dynamics & Earthquake Engineering*, Vol. 27, pp. 200-211

[13] Liu, M., Wang, Y.-Y., and Yu, Z., (2008), "Response of pipelines under fault crossing.", *Proceedings, International Offshore and Polar Engineering Conference*, Vancouver, BC, Canada.

[14] Ha, D., Abdoun T. H., O'Rourke, M. J., Symans, M. D., O'Rourke, T. D., Palmer, M. C., Stewart, H. E. (2008), "Buried high-density polyethylene pipelines subjected to normal and strike-slip faulting – a centrifuge investigation.", *Canadian Geotechnical Journal*, Vol. 45, pp. 1733-1742.

[15] Ha, D., Abdoun T. H., O'Rourke, M. J., Symans, M. D., O'Rourke, T. D., Palmer, M. C., Stewart, H. E. (2008), "Centrifuge Modeling of Earthquake Effects on Buried High-Density Polyethylene (HDPE) Pipelines Crossing Fault Zones.", *ASCE Journal of Geotechnical and Geoenvironmental Engineering*, Vol. 134, No. 10, pp. 1501-1515.

[16] Abdoun T. H., Ha, D., O'Rourke, M. J., Symans, M. D., O'Rourke, T. D., Palmer, M. C., Stewart, H. E. (2009), "Factors influencing the behavior of buried pipelines subjected to earthquake faulting.", *Soil Dynamics and Earthquake Engineering*, Vol. 29, pp. 415– 427.

[17] Lillig D. B., Newbury B. D. and Altstadt S. A. (2009), "The Second ISOPE Strain-Based Design Symposium - A Review.", *International Society of Offshore & Polar Engineering Conference*, Osaka, Japan.

[18] ABAQUS (2008): *Users' Manual*, *Version 6.7*, Simulia, Providence, RI, USA.

[19] Anastasopoulos, I., Callerio, A., Bransby, M. F., Davies, M. C., Nahas, A. El, Faccioli, E., Gazetas, G., Masella, A., Paolucci, R., Pecker, A., Rossigniol, E. (2008), "Numerical analyses of fault foundation interaction.", *Bulletin of Earthquake Engineering*, Springer, 6(4), 645-675.

[20] American Petroleum Institute (2007), *Specification for Line Pipe*, 44th Edition, ANSI/API Spec 5L.

[21] American Society of Mechanical Engineers (2007), *Gas Transmission and Distribution Piping Systems*, ANSI/ASME B31.8.

[22] Igi, S. and Suzuki, N. (2007), "Tensile Strain Limits of X80 High-strain Pipelines.", *Proceedings of the 16th International Offshore and Polar Engineering Conference*, Lisbon, Portugal.

[23] Dama, E., Karamanos, S. A. and Gresnigt, A. M. (2007), "Failure of Locally Buckled Pipelines.", *Journal of Pressure Vessel Technology*, ASME, Vol. 129, pp. 272-279.

[24] Gresnigt, A. M. and Karamanos, S. A. (2009), "Local Buckling Strength and Deformation Capacity of Pipes.", *19th International Offshore and Polar Engineering Conference*, Osaka, Japan, pp. 212-223.

[25] Gresnigt, A. M., (1986), "Plastic Design of Buried Steel Pipelines in Settlement Areas", *Heron*, Vo. 31, No. 4, Delft, The Netherlands.

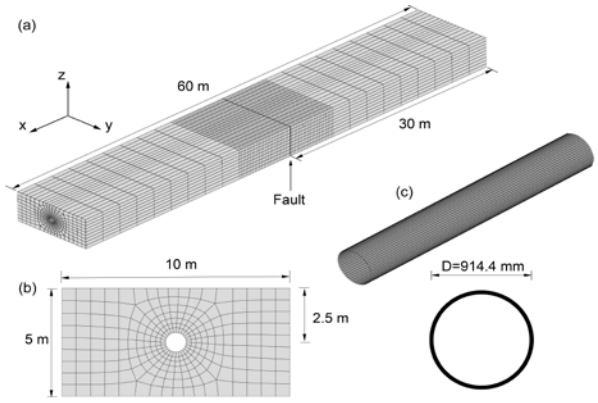

Figure 1: Finite element model of the (a) soil formation with tectonic fault, (b) soil cross-section and (c) steel pipeline.

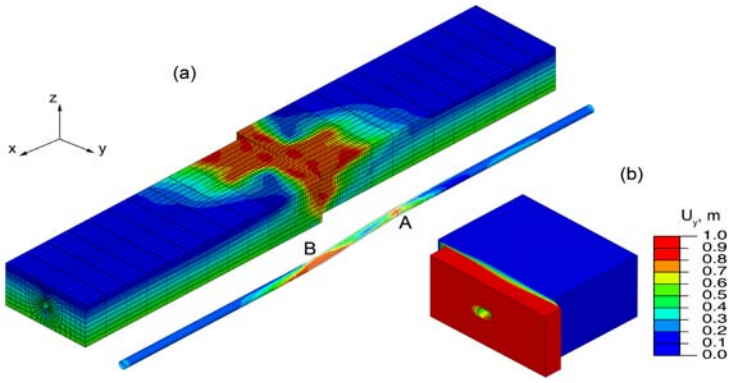

Figure 2: (a) Deformation of the pipeline-soil system after fault displacement; finite element results depict the von Mises stress. (b) Detail of fault displacement U_y (X65 pipe, $D/t = 72$, Clay I, $w = 0.33$ m, $p = 0$).

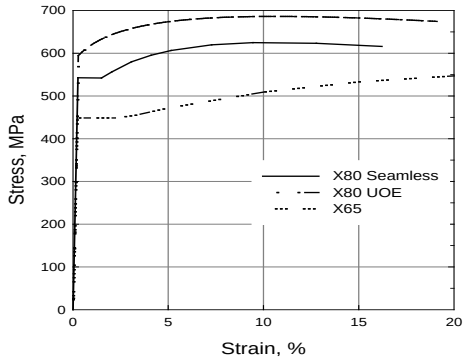

Figure 3: Uniaxial nominal stress-engineering strain curve for API 5L X65 , API 5L X80 steel.

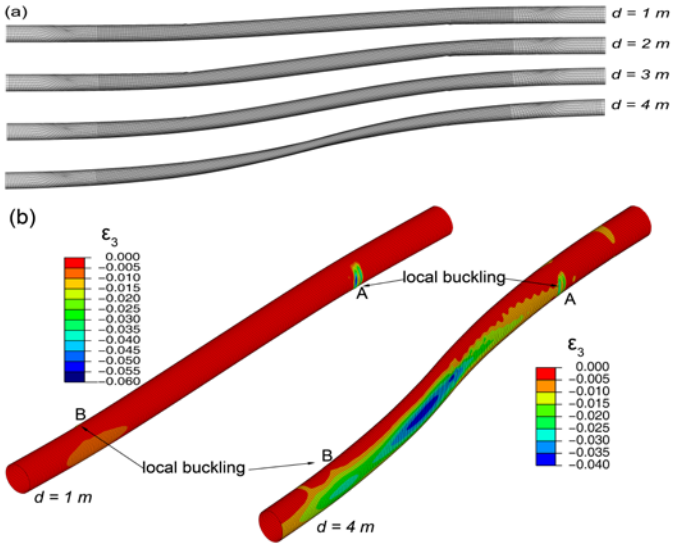

Figure 4: (a) Plan view of deformed shape of a pipeline for d = 1, 2, 3, and 4 m (b) Distribution of longitudinal normal strain ε_x for seismic fault displacement equal to 1 m and 4 m. (X65 pipe, $D/t = 72$, Clay I, $w = 0.33$ m, $p = 0$).

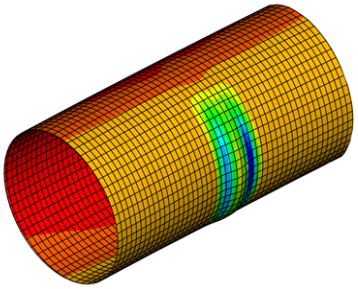

Figure 5: Details of the critical pipeline area: local buckling formation (X65 pipe, $D/t = 72$, Clay I, $w = 0.33$m, $p = 0$).

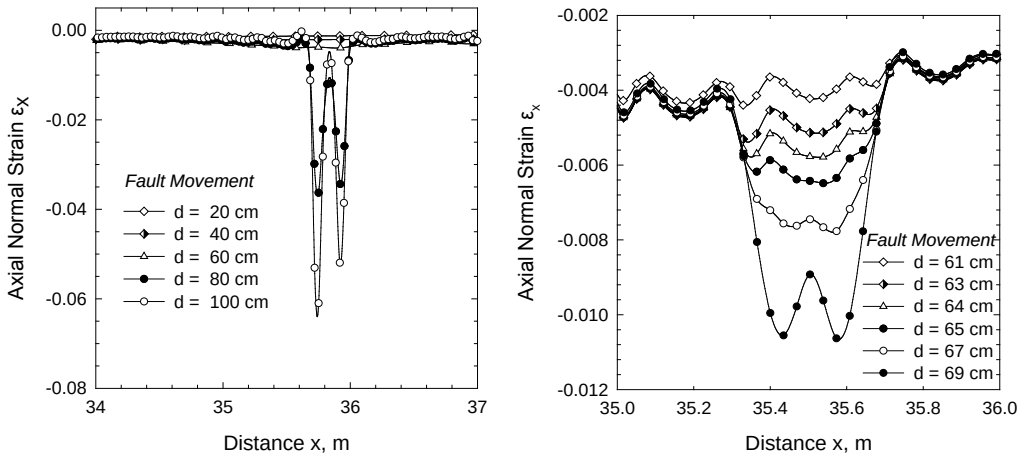

Figure 6: Variation of axial strain at the compression side of the buckled area for different values of fault displacement: (a) fault movement from 0.2m to 1.0m and (b) fault movement from 0.61m to 0.69m (X65 pipe, $D/t = 72$, Clay I, $w = 0.33$m, $p = 0$).

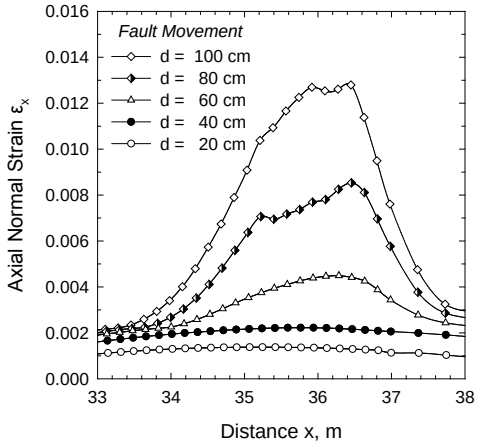

Figure 7: Variation of axial strain at the tension side of the buckled area for values of fault displacement from 0.2m to 1.0m (X65 pipe, $D/t = 72$, Clay I, $w = 0.33$m, $p = 0$).

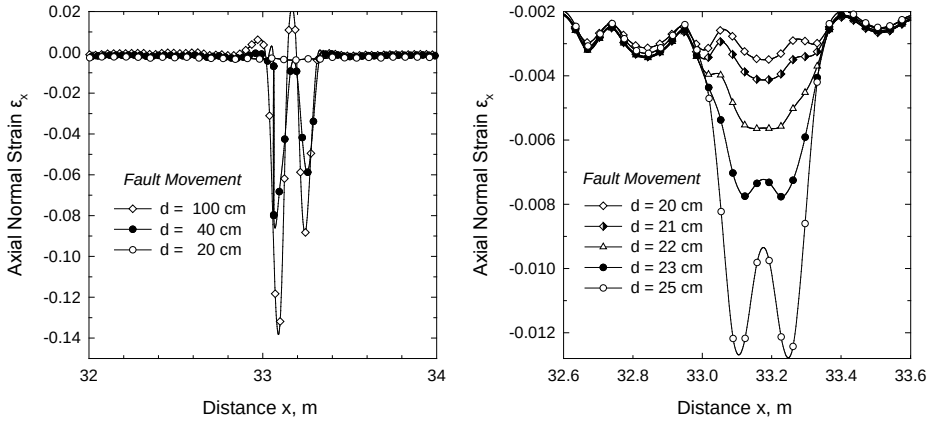

Figure 8: Variation of axial strain at the compression side of the buckled area for different values of fault displacement: (a) fault movement from 0.2m to 1.0m and (b) fault movement from 0.20m to 0.25m (X65 pipe, $D/t = 72$, Clay II, $w = 0.33$m, $p = 0$).

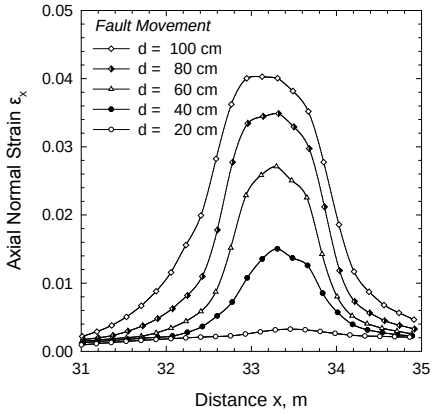

Figure 9: Variation of axial strain at the tension side of the buckled area in terms of fault displacement from 0.2m to 1.0m (X65 pipe, $D/t = 72$, Clay II, $w = 0.33$m, $p = 0$).

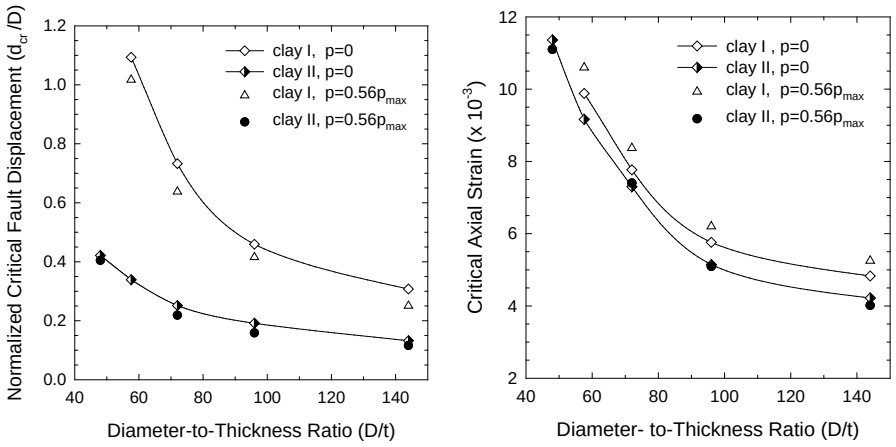

Figure 10: (a) Critical fault movement versus the diameter-to-thickness ratio D/t for clay I, II and (b) Critical axial strain versus the diameter-to-thickness ratio D/t for clay I, II (X65 pipe, $w = 0.33$m, $p = 0$ and $p = 0.56\,p_{\max}$).

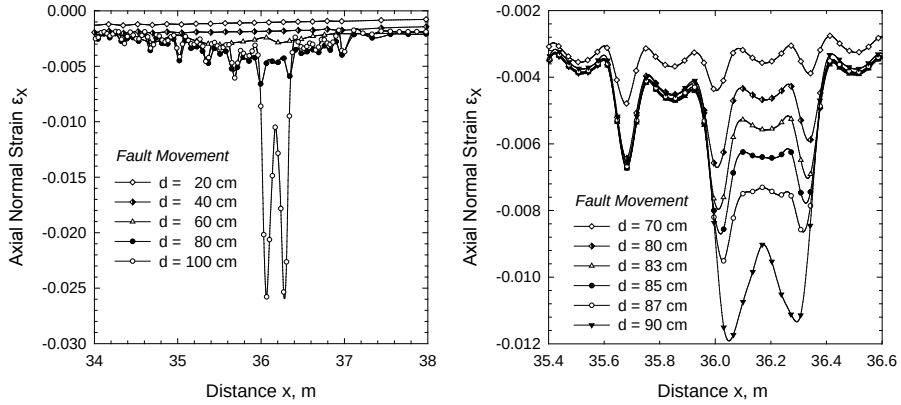

Figure 11: Variation of axial strain at the compression side of the buckled area for different values of fault displacement (a) fault movement from 0.2m to 1.0m and (b) fault movement from 0.70m to 0.90m (X65 pipe, $D/t = 72$, Sand I, $w = 0.33$m, $p = 0$).

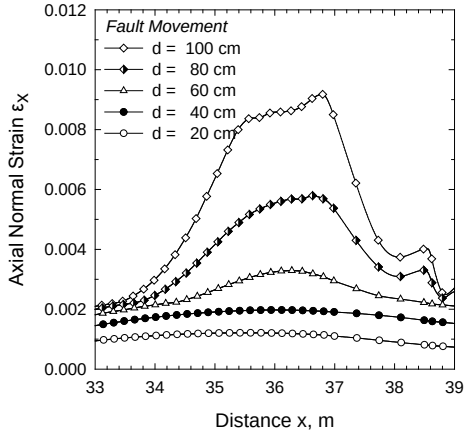

Figure 12: Variation of axial strain at the tension side of the buckled area for different values of fault displacement from 0.2m to 1.0m (X65 pipe, $D/t = 72$, Sand I, $w = 0.33$m, $p = 0$).

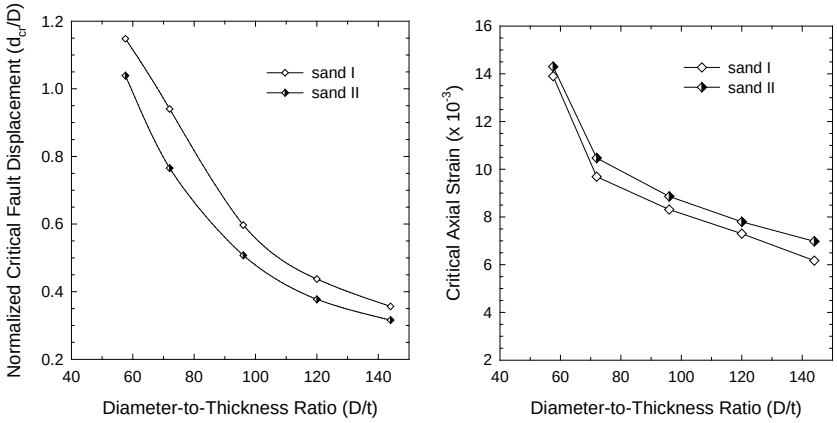

Figure 13: (a) Critical fault movement versus the diameter-to-thickness ratio D/t for sand I, II and (b) Critical axial strain versus the diameter-to-thickness ratio D/t for sand I, II (X65 pipe, $w = 0.33\text{m}$, $p = 0$).

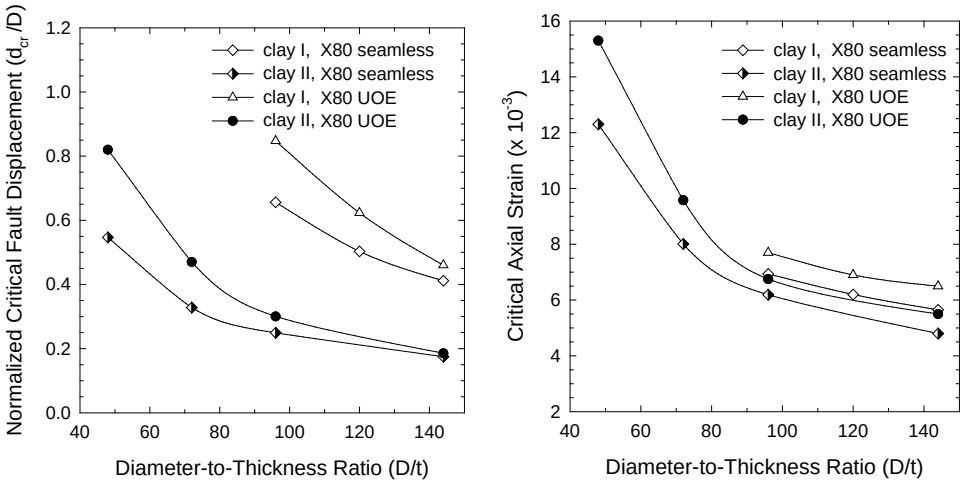

Figure 14: (a) Critical fault movement versus the diameter-to-thickness ratio D/t for two different types of X80 pipelines and (b) Critical axial strain versus the diameter-to-thickness ratio D/t for two different types of X80 (X80 pipe, $w = 0.33\text{m}$, $p = 0$)

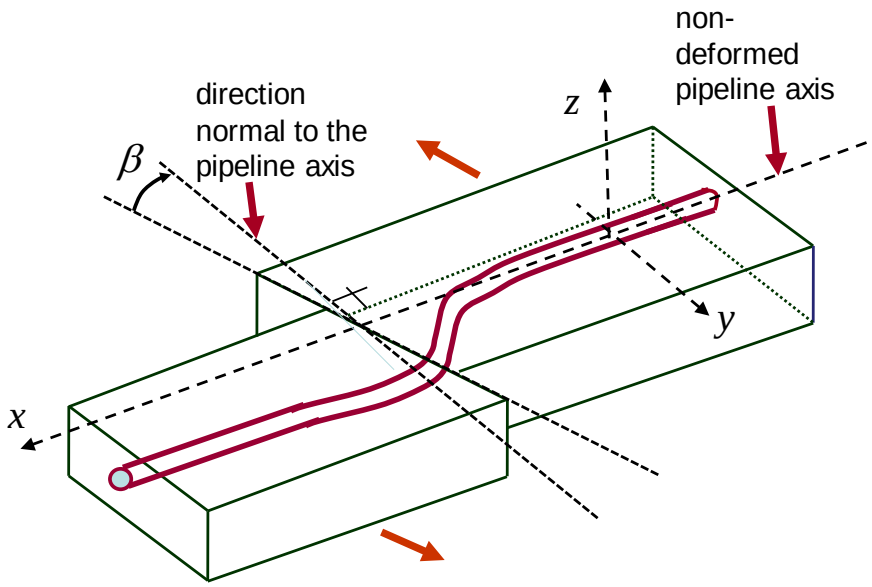

Figure 15: Schematic representation of a pipeline crossing a strike-slip fault at a certain angle.

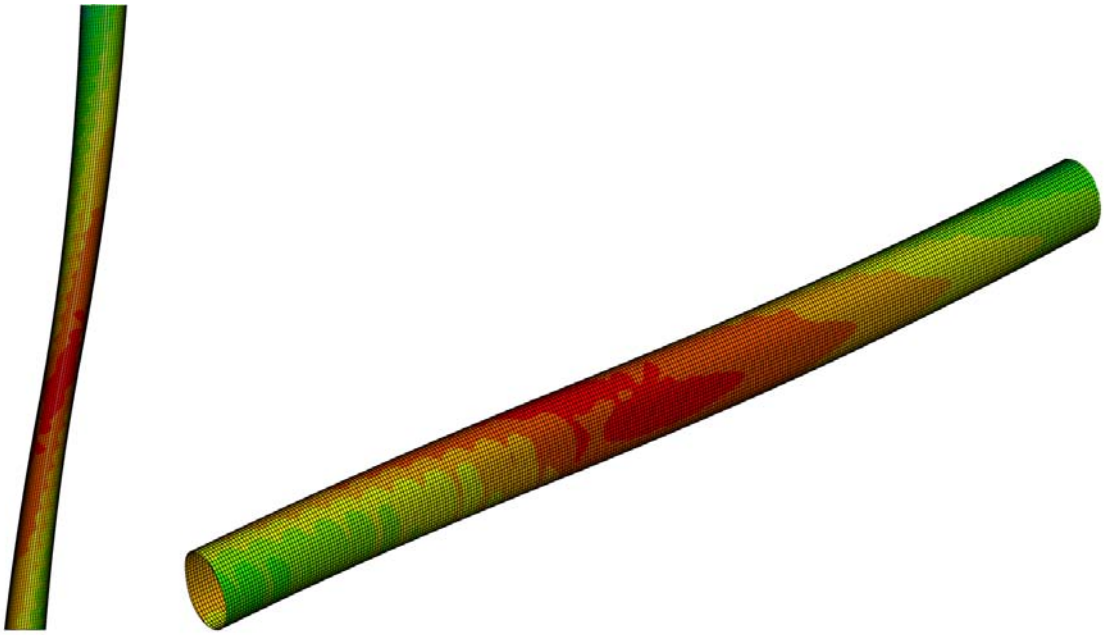

Figure 16: Deformed shape of the pipeline for β =25 degrees, at a fault displacement d = 2 m; top view (left) and three-dimensional view (right).

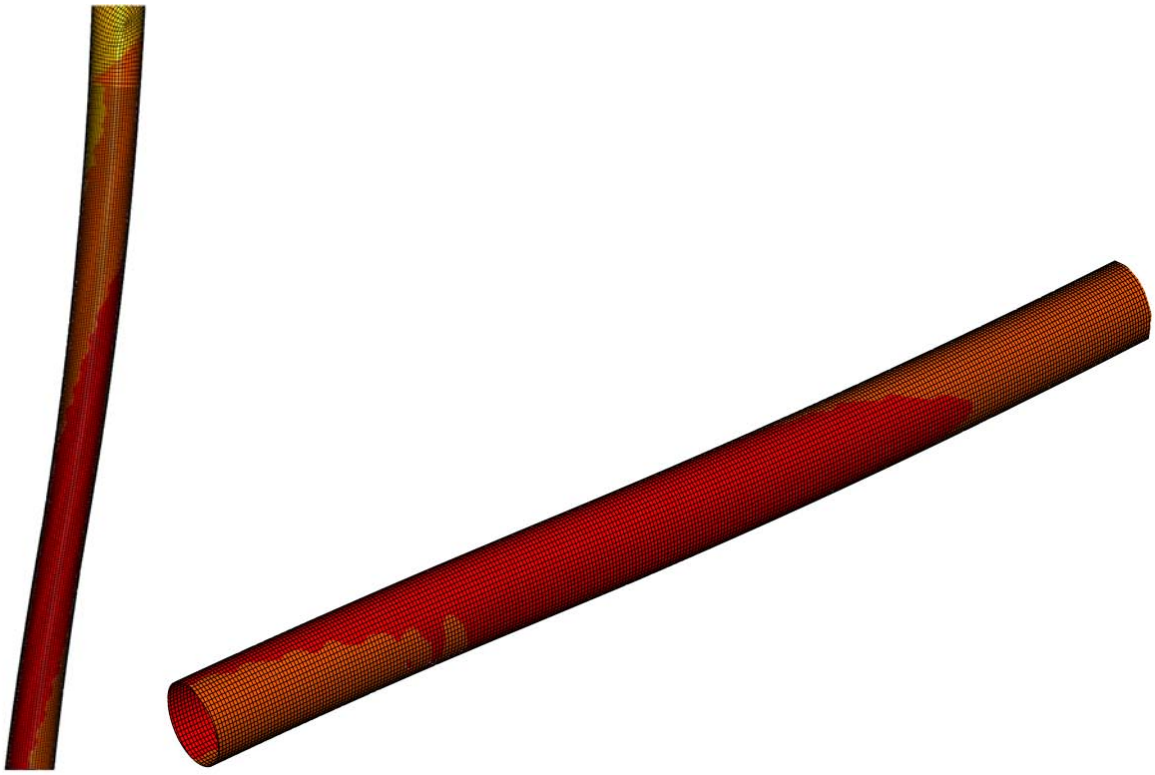

Figure 17: Deformed shape of the pipeline for β = 45 degrees, at d = 2 m; top view (left) and three-dimensional view (right).

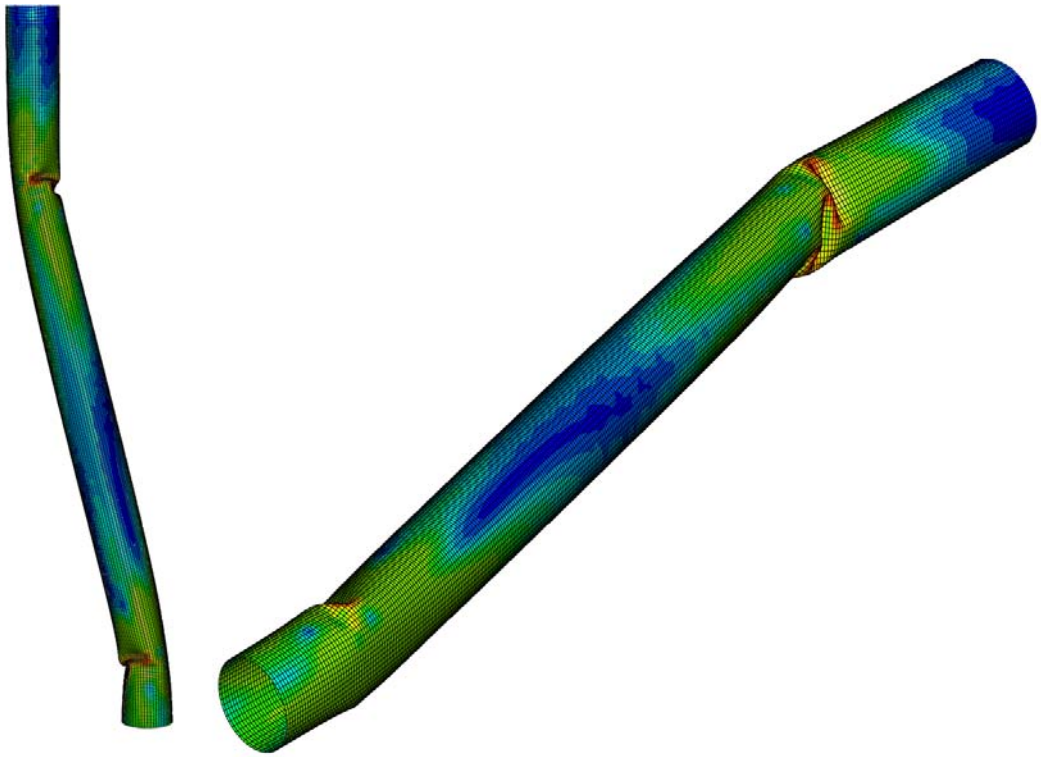

Figure 18: Deformed shape of the pipeline for β = -10 degrees, at d = 2 m; top view (left) and three-dimensional view (right).